TECHNISCHE MECHANIK
an open access journal

journal homepage: www.ovgu.de/techmech

Tech. Mech., Vol. 42, Is. 1, (2022), 1–13

Received: 22.02.2022
Accepted: 28.04.2022
Available online: 02.05.2022

Nonlinear Low-Velocity Impact Response of Carbon Fiber-Epoxy Reinforced Nanocomposite Plates Using Finite Element Method

R. Selvamani and J. Nicholas George

Department of Mathematics, Karunya Institute of Technology and Sciences, Coimbatore - 641 114, Tamilnadu, India

Abstract: In this study, the effect of addition of carbon nanotube on the nonlinear low-velocity impact response of carbon fiber/epoxy composites is performed using the finite element method. The effective material properties of the multiscale composites are calculated using Halpin-Tsai equations and fiber micromechanics in hierarchy. The governing equations are derived based on higher-order shear deformation plate theory(HSDT) and von Kármán geometrical nonlinearity. The carbon nanotubes are assumed to be uniformly distributed and randomly oriented through the epoxy resin matrix. Contact force between the impactor and the plate is obtained with the aid of the modified nonlinear Hertzian contact law models. After examining the validity of the present work, the effects of the weight percentage of single-walled carbon nanotubes(SWCNTs) and multi-walled carbon nanotubes(MWCNTs), nanotube aspect ratio, volume fraction of fibers, plate aspect ratio and initial velocity of the impactor on the contact force, indentation, and central deflection of CNT reinforced multi-phase laminated composite plate are studied in detail.

Keywords: Carbon fiber, Nano-structures, Impact behavior, Finite element analysis (FEA).

1 Introduction

Owing to the unique properties, carbon fiber reinforced composites are proper substitutes for traditional metals. Some mechanical properties such as high strength to weight ratio, fatigue and wear resistance and formability of intricate shapes increase a widespread use of composites in industries such as aerospace, automotive and military in which weight plays an important role. To the best of author's knowledge, there is no theoretical analysis on the impact resistance of CNTs/fiber/polymer multi-phase composites carried out till now. The high susceptibility of damage to impact is one of the major concerns of CFRP composite structures Rahman et al. (2015); Thostenson et al. (2001). In this regard, improving the impact resistance becomes an important issue considering the critical applications of these materials. For improvement of the multi functionality of fiber-reinforced composites, CNTs are an excellent candidate for nanoscale reinforcement. Their elastic modulus of over 1 TPa and tensile strength of over 150 GPa make them much stiffer and stronger than steel while being three to five times lighter Kim et al. (2009). Research groups have demonstrated that mechanical properties of composites can be strongly increased by adding a few weight percent (wt. %) of either single or multi-walled carbon nanotubes Spitalsky et al. (2010); Sahoo et al. (2010).

A research on the development of advanced structural composites based on engineered CNTs/fiber/polymer multiscale composites presented by Bekyarova et al. (2007); Kim et al. (2009) fabricated and characterized the CFRP composites modified with CNTs via high-energy sonication. Thostenson et al. (2002) studied the effect of local nanotube reinforcement on load transfer at the fiber/matrix interface of CNTs/fiber/polymer multiscale composites. Godara et al. (2009) investigated the effect of CNT reinforcement on the processing and the mechanical behavior of CFRP composites. The CNT dispersion and its stability during the processing steps and the final mechanical properties of composites are discussed in detail in their study. Green et al. (2009) studied synthesis, mechanical, and thermo-mechanical behavior of carbon nano fiber/epoxy nano phased polymer matrix. Akgoz and Civalek (2013) analyzed the buckling analysis of cantilever carbon nanotubes using the strain gradient elasticity and modified couple stress theory. They concluded that the classical theory and modified couple stress theories are inappropriate to model the buckling of CNT with smaller diameter even at higher modes.

Rafiee et al. (2014b) presented nonlinear free vibration of CNT/fiber/polymer multiscale laminated composite plates integrated with piezoelectric layer. By using an analytical approach, Rafiee et al. (2014a) carried out modeling and stress analysis of smart CNTs/fiber/polymer composite plates. Nonlinear flexural and dynamic response of CNT reinforced laminated composite plates are analyzed by Bhardwaj et al. (2012). They used double Chebyshev polynomials to solve the problem. He et al. (2015) investigated large amplitude vibration of fractionally damped viscoelastic CNTs/fiber/polymer multiscale composite beams.

A few studies have addressed the effects of CNTs on low-velocity impact of CFRP composites. Kostopoulos et al. (2010) investigated the effect of MWCNTs on the impact and after impact behavior of carbon fiber reinforced polymer(CFRP). They observed enhanced impact damage resistance at 0.5 wt.% CNT doped specimens and also, the post impact properties after impact were improved for all CNT infused specimens compared with the control specimen. Soliman et al. (2012) presented the low-velocity-impact response of thin carbon woven fabric composites reinforced with different weight percentages of MWCNTs. It was observed that the MWCNTs enhanced the impact response, limited the damage size and energy absorption in the woven carbon fiber composites. In all of these interesting works, experimental methods were carried out.

* E-mail address: selvam1729@gmail.com
doi: 10.24352/UB.OVGU-2022-057

Furthermore found that, a limited number of research works available theoretically/numerically on the low-velocity impact of the CNT reinforced composite (CNTRC). However, all of these studies are performed for two-phase CNT-reinforced polymeric composites. Rafiee and Moghadam (2012) simulated the impact and post-impact behavior of nanotube-reinforced polymer based on a multi-scale finite element model software. Their results showed that the deflection of the composite with adding only 5% volume fraction of CNT was much smaller than that of neat resin. Jam and Kiani (2015) presented the response of FGCNTRC beams under low velocity impact based on the first order beam theory. Equivalent properties of the composite media are estimated by applying a refined rule of mixture approach. Wang et al. (2014) analyzed the nonlinear low velocity impact response of temperature-dependent nanotube-reinforced composite plates under thermal loading by applying the rule of mixture. They used a two-step perturbation technique to solve the problem for simply supported plates.

Ebrahimi et al. (2020a) analyzed the thermal buckling analysis of magneto electro elastic porous FG beam in thermal environment. Ebrahimi et al. (2020b) developed the bending analysis of magneto-electro piezoelectric nanobeams system under hygro-thermal loading. Ebrahimi et al. (2020c) studied the dynamic characteristics of hygro-magneto-thermo-electrical nanobeam with non-ideal boundary conditions. Ebrahimi et al. (2020d) reported the thermo-electro-elastic nonlinear stability analysis of viscoelastic double-piezo nanoplates under magnetic field. Selvamani and Ebrahimi (2020) investigated the axisymmetric vibration in a submerged, piezoelectric rod coated with thin film. Ebrahimi et al. (2015) reported the thermo mechanical vibration behavior of FG nanobeams subjected to linear and non-linear temperature distributions. Demir et al. (2016) studied the determination of critical buckling loads of isotropic, FGM and laminated truncated conical panel, they concluded from the results that the critical buckling load of the laminated panels increase with increasing number of layers. Talebitooti (2013) developed the three-dimensional free vibration analysis of rotating laminated conical shells: layerwise differential quadrature (LW-DQ) method. Akgoz and Civalek (2013) reported the vibration analysis of micro-scaled sector shaped graphene surrounded by an elastic matrix, they found that the frequency values increase with an increase of Winkler and Pasternak elastic foundation parameters. Gurses et al. (2009) analyzed the free vibration analysis of symmetric laminated skew plates by discrete singular convolution technique based on first-order shear deformation theory.

In the present study, the influence of single-walled carbon nanotubes (SWCNTs) and multi-walled carbon nanotubes (MWCNTs) on the nonlinear low-velocity impact response of carbon fiber/epoxy composites using the finite element method is performed. In this regard, the governing equations are derived based on higher-order shear deformation plate theory (HSDT) and von Kármán geometrical nonlinearity. The considered element is C^1-continuous with 15 DOF at each node. The effective material properties of the multiscale composite are calculated using Halpin-Tsai equations and fiber micromechanics in hierarchy. The carbon nanotubes are assumed to be uniformly distributed and randomly oriented through the epoxy resin matrix. Contact force between the impactor and the plate is obtained with the aid of the modified nonlinear Hertzian contact law models. After examining the validity of the present work, the effects of the weight percentage of SWCNTs and MWCNTs, nanotube aspect ratio, volume fraction of fibers, plate aspect ratio and initial velocity of the impactor on the contact force, indentation, and central deflection of CNT reinforced multi-phase laminated composite plate are studied in detail.

2 Theoretical formulation

2.1 Carbon nanotube/fiber/polymer multi-phase composite material model

Consider a rectangular laminated composite plate composed of isotropic matrix (epoxy resin), CNTs and fibers (carbon) impacted by a low-velocity spherical impactor whose initial velocity and radius are denoted by V_0 and R, respectively (Fig. 1). The geometric parameters and the coordinate system used for the plate and the impactor are shown in Fig. 1.

The effective mechanical properties of these composites can be obtained based on micromechanics approach scheme (Shen (2009)), via two steps in the hierarchy as shown in Fig. 2. The resulting effective properties of the CNT reinforced multi-phase laminated composite plate are orthotropic and can be expressed as on Shen (2009):

$$E_{11} = V_F E_{11}^F + V_{MNC} E^{MNC} \tag{1}$$

$$\frac{1}{E_{22}} = \frac{1}{E_{22}^F} + \frac{V_{MNC}}{E^{MNC}} - V_F V_{MNC} - \frac{\frac{\nu_F^2 E^{MNC}}{E_{22}^F} + \frac{\nu_{MNC}^2 E_{22}^F}{E^{MNC}} - 2\nu^F \nu^{MNC}}{V_F E_{22}^F + V_{MNC} E^{MNC}} \tag{2}$$

$$\frac{1}{G_{12}} = \frac{V_F}{G_{12}^F} + \frac{V_{MNC}}{G^{MNC}} \tag{3}$$

$$\rho = V_F \rho^F + \frac{V_{MNC}}{\rho^{MNC}} \tag{4}$$

$$\nu_{12} = V_F \nu^F + V_{MNC} \nu^{MNC} \tag{5}$$

where E, G, ν, V and ρ denote the moduli, shear modulus, Poisson's ratio, volume fractions and mass density, respectively, while the superscript or subscript F and MNC signify the fibers and matrix of nanocomposite, respectively.

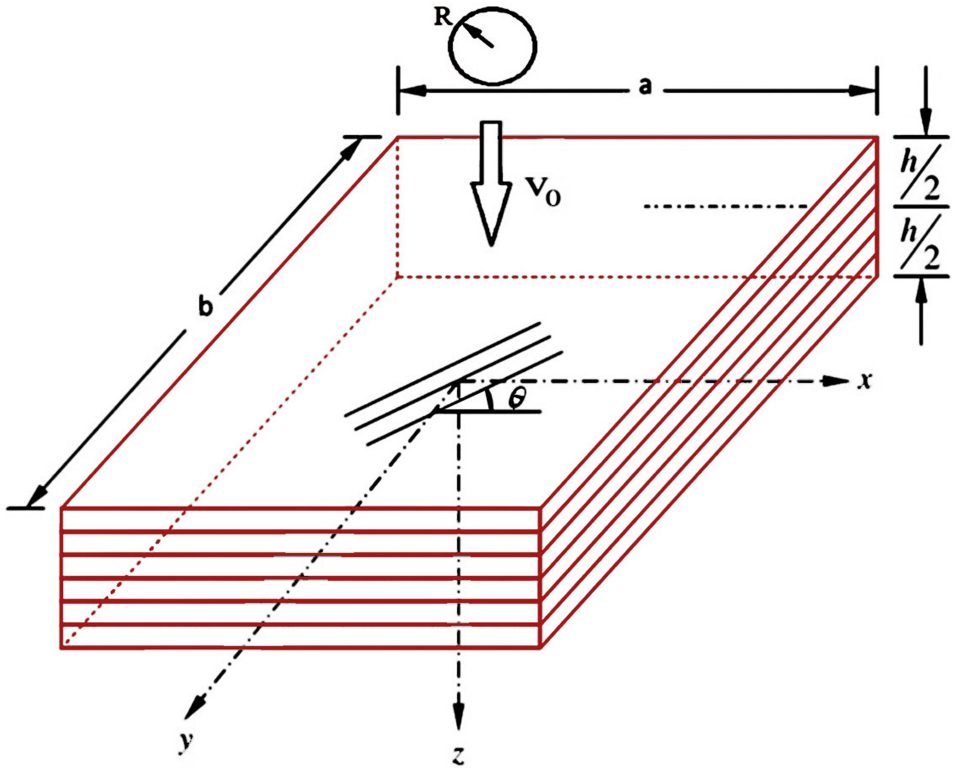

Fig. 1: The geometric parameters CNT reinforced multi-phase laminated composite plate

Based on the Halpin-Tsai model, the tensile modulus of nanocomposites can be expressed as:

$$E^{MNC} = \frac{E^M}{8}\left[5\left(\frac{1+2\beta_{dd}V_{CN}}{1-\beta_{dd}V_{CN}}\right)+3\left(\frac{1+2(\ell^{CN}/d^{CN})\beta_{dl}V_{CN}}{1-\beta_{dl}V_{CN}}\right)\right] \tag{6}$$

$$\beta_{dl} = \frac{(E_{11}^{CN}/E^M)-(d^{CN}/4t^{CN})}{(E_{11}^{CN}/E^M)+(\ell^{CN}/2t^{CN})} \tag{7}$$

$$\beta_{dd} = \frac{(E_{11}^{CN}/E^M)-(d^{CN}/4t^{CN})}{(E_{11}^{CN}/E^M)+(d^{CN}/2t^{CN})} \tag{8}$$

where E^{CN}, V_{CN}, ℓ^{CN}, d^{CN} and t^{CN} are the Young's modulus, volume fraction, length, outer diameter and the thickness of carbon nanotubes, respectively, and V_M and E^M indicate the volume fraction and Young's modulus of the isotropic epoxy resin matrix, respectively. The volume fraction of carbon nanotubes may be defined as (Rafiee et al. (2013)):

$$V_{CN} = \frac{w_{CN}}{w_{CN}+\left(\frac{\rho^{CN}}{\rho^M}\right)-\left(\frac{\rho^{CN}}{\rho^M}\right)w_{CN}} \tag{9}$$

where w_{CN} is the mass fraction of the carbon nanotubes, ρ^{CN} and ρ^M are the mass densities of the carbon nanotube and epoxy resin matrix, respectively. The Poisson's ratio and mass density ρ can be expressed as:

$$\upsilon^{MNC} = \upsilon^M \tag{10}$$

$$\rho^{MNC} = V_{CN}\rho^{CN} + V_M\rho^M \tag{11}$$

where υ^M is Poisson's ratio of the epoxy resin matrix. Since that the amount of CNTs was small, υ^{MNC} was considered to be the same as that of epoxy.

2.2 Impact dynamics and contact law

For low velocity impact on laminates the contact force F_c can be related to the indentation α by applying the modified nonlinear Hertz contact law as (Mura (1987)):

$$F_c = k_c\alpha^{3/2} \tag{12}$$

where k_c is the modified Hertz contact stiffness proposed by Sun and Chen (1985) as:

$$k_c = \frac{4}{3} E^* R_i^{1/2} \tag{13}$$

with:

$$\frac{1}{E^*} = \frac{1 - v_i^2}{E_i} + \frac{1}{E_{22}} \tag{14}$$

where R_i, E_i and v_i are the radius, Young's modulus and Poisson's ratio of the impactor, respectively and E_{22} is the transverse modulus of the surface of the composite lamina.
During the unloading and subsequent reloading, the contact force F_c can be defined respectively (Yang and Sun (1982)):

$$\begin{aligned} F_c &= F_m \left[(\alpha - \alpha_0)/(\alpha_m - \alpha_0)\right]^{5/2} \\ F_c &= F_m \left[(\alpha - \alpha_0)/(\alpha_m - \alpha_0)\right]^{3/2} \end{aligned} \tag{15}$$

where F_m and α_m are the maximum contact force and local indentation during the loading phase, respectively. The permanent indentation α_0 equals to zero when α_m remains below a critical indentation(Yang and Sun (1982)).

2.3 Displacement field model

According to the higher order shear-deformation theory (Reddy (2004)), the displacement field of laminated plate theory can be expressed as:

$$u(x, y, z, t) = u_0(x, y, t) + z\phi_x - c_1 z^3 \left(\phi_x + \frac{\partial w_0}{\partial x}\right); \tag{16}$$

$$v(x, y, z, t) = v_0(x, y, t) + z\phi_y - c_1 z^3 \left(\phi_y + \frac{\partial w_0}{\partial y}\right); \tag{17}$$

$$w(x, y, z, t) = w_0(x, y, t) \tag{18}$$

here u_0, v_0, and w_0 denote the displacements at the mid-plane of the reference plane of the plate and ϕ_x and ϕ_y are rotations about the y and x axes, respectively and $c_1 = 4/3h^2$. This shear theory is based on the concept that the transverse shear strain and hence shear stress vanish on the top and bottom surfaces of the plate and are nonzero elsewhere. So, a shear correction factor is not required. The strain-displacement relations, based on von Kármán's large deformation assumption are:

$$\left\{ \begin{array}{c} \varepsilon_{xx} \\ \varepsilon_{yy} \\ \gamma_{xy} \end{array} \right\} = \varepsilon_0 + z\varepsilon_1 + z^3\varepsilon_3, \quad \left\{ \begin{array}{c} \gamma_{yz} \\ \gamma_{xz} \end{array} \right\} = \gamma_0 + z^2\gamma_2 \tag{19}$$

where:

$$\varepsilon_0 = \left\{ \begin{array}{c} \frac{\partial u_0}{\partial x} + \frac{1}{2}\left(\frac{\partial w_0}{\partial x}\right)^2 \\ \frac{\partial v_0}{\partial y} + \frac{1}{2}\left(\frac{\partial w_0}{\partial y}\right)^2 \\ \frac{\partial u_0}{\partial y} + \frac{\partial v_0}{\partial x} + \frac{\partial w_0}{\partial x}\frac{\partial w_0}{\partial y} \end{array} \right\}, \quad \varepsilon_1 = \left\{ \begin{array}{c} \frac{\partial \phi_x}{\partial x} \\ \frac{\partial \phi_y}{\partial y} \\ \frac{\partial \phi_x}{\partial y} + \frac{\partial \phi_y}{\partial x} \end{array} \right\}, \quad \varepsilon_3 = -c_1 \left\{ \begin{array}{c} \frac{\partial \phi_x}{\partial x} + \frac{\partial^2 w_0}{\partial x^2} \\ \frac{\partial \phi_y}{\partial y} + \frac{\partial^2 w_0}{\partial y^2} \\ \frac{\partial \phi_x}{\partial y} + \frac{\partial \phi_y}{\partial x} + 2\frac{\partial^2 w_0}{\partial x \partial y} \end{array} \right\},$$
$$\gamma_0 = \left\{ \begin{array}{c} \frac{\partial w_0}{\partial x} + \phi_x \\ \frac{\partial w_0}{\partial y} + \phi_y \end{array} \right\}, \quad \gamma_0 = -c_2 \left\{ \begin{array}{c} \frac{\partial w_0}{\partial x} + \phi_x \\ \frac{\partial w_0}{\partial y} + \phi_y \end{array} \right\} \tag{20}$$

In the above relations, ε_{xx}, ε_{yy} and $\gamma_{\mathbf{xy}}$ denote in-plane strains, γ_{yz} and γ_{xz} are transverse shear strains and $c_2 = 3c_1$. The governing equations can be generated by applying principle of virtual work (Setoodeh et al. (2009)):

$$\begin{aligned} &\int_{-\frac{h}{2}}^{\frac{h}{2}} \int_0^b \int_0^a \{\delta\varepsilon\}^T \{\sigma\} dxdydz \\ &\qquad + \int_{-\frac{h}{2}}^{\frac{h}{2}} \int_0^b \int_0^a \rho \{\mathbf{u}\delta u + \mathbf{v}\delta v + \mathbf{w}\delta w\} dxdydz - \int_0^b \int_0^a q\delta w dxdy - F_c \delta\alpha = 0 \end{aligned} \tag{21}$$

2.4 Constitutive equations

The constitutive relation of the k^{th} layer of the laminate in the material axes can be stated as Sun and Hsu (1990):

$$\begin{Bmatrix} \sigma_1 \\ \sigma_2 \\ \tau_{23} \\ \tau_{31} \\ \tau_{12} \end{Bmatrix} = \begin{bmatrix} Q_{11} & Q_{12} & 0 & 0 & 0 \\ Q_{12} & Q_{22} & 0 & 0 & 0 \\ 0 & 0 & Q_{44} & 0 & 0 \\ 0 & 0 & 0 & Q_{55} & 0 \\ 0 & 0 & 0 & 0 & Q_{66} \end{bmatrix} \left(\begin{Bmatrix} \varepsilon_1 \\ \varepsilon_2 \\ \gamma_{23} \\ \gamma_{31} \\ \gamma_{12} \end{Bmatrix} - \begin{Bmatrix} \alpha_{11} \\ \alpha_{22} \\ 0 \\ 0 \\ 0 \end{Bmatrix} \Delta T \right) \tag{22}$$

where:

$$\begin{gathered} Q_{11} = \frac{E_{11}}{1 - v_{12}v_{21}}, \quad Q_{66} = G_{12}, \quad Q_{22} = \frac{E_{22}}{1 - v_{12}v_{21}}, \quad Q_{44} = G_{23}, \\ Q_{12} = \frac{v_{12}E_{22}}{1 - v_{12}v_{21}}, \quad Q_{55} = G_{13}, \end{gathered} \tag{23}$$

E_{11} and E_{22} are the Young's modulus of CNTRC plates in the principle material coordinates G_{12}, G_{13} and G_{23} are the shear modulus; and ΔT is the temperature change with respect to a reference state.
If the fiber angle with the geometric x axis is denoted by θ, the relation (22) can be transferred to the geometric coordinates as:

$$\begin{Bmatrix} \sigma_x \\ \sigma_y \\ \tau_{yz} \\ \tau_{xz} \\ \tau_{xy} \end{Bmatrix}_k = \begin{bmatrix} \overline{Q}_{11} & \overline{Q}_{12} & 0 & 0 & \overline{Q}_{16} \\ \overline{Q}_{12} & \overline{Q}_{22} & 0 & 0 & \overline{Q}_{26} \\ 0 & 0 & \overline{Q}_{44} & \overline{Q}_{45} & 0 \\ 0 & 0 & \overline{Q}_{45} & \overline{Q}_{55} & 0 \\ \overline{Q}_{16} & \overline{Q}_{26} & 0 & 0 & \overline{Q}_{66} \end{bmatrix}_k \left(\begin{Bmatrix} \varepsilon_x \\ \varepsilon_y \\ \gamma_{yz} \\ \gamma_{xz} \\ \gamma_{xy} \end{Bmatrix} - \begin{Bmatrix} \alpha_{11} \\ \alpha_{22} \\ 0 \\ 0 \\ 0 \end{Bmatrix} \Delta T \right)_k \tag{24}$$

where:

$$\overline{Q}_{11} = Q_{11}\cos^4\theta + 2(Q_{12} + 2Q_{66})\sin^2\theta\cos^2\theta + Q_{22}\sin^4\theta, \tag{25}$$
$$\overline{Q}_{12} = (Q_{11} + Q_{22} - 4Q_{66})\sin^2\theta\cos^2\theta + Q_{12}(\sin^4\theta + \cos^4\theta), \tag{26}$$
$$\overline{Q}_{22} = Q_{11}\sin^4\theta + 2(Q_{12} + 2Q_{66})\sin^2\theta\cos^2\theta + Q_{22}\cos^4\theta, \tag{27}$$
$$\overline{Q}_{16} = (Q_{11} - Q_{12} - 2Q_{66})\sin\theta\cos^3\theta + (Q_{12} - Q_{22} + 2Q_{66})\sin^3\theta\cos\theta, \tag{28}$$
$$\overline{Q}_{26} = (Q_{11} - Q_{12} - 2Q_{66})\sin^3\theta\cos\theta + (Q_{12} - Q_{22} + 2Q_{66})\sin\theta\cos^3\theta, \tag{29}$$
$$\overline{Q}_{66} = (Q_{11} + Q_{22} - 2Q_{12} - 2Q_{66})\sin^2\theta\cos^2\theta + Q_{66}(\sin^4\theta + \cos^4\theta), \tag{30}$$
$$\overline{Q}_{44} = Q_{44}\cos^2\theta + Q_{55}\sin^2\theta, \tag{31}$$
$$\overline{Q}_{45} = (Q_{55} - Q_{44})\cos\theta\sin\theta, \tag{32}$$
$$\overline{Q}_{55} = Q_{55}\cos^2\theta + Q_{44}\sin^2\theta \tag{33}$$

3 Finite element formulation

In present section, the equations of HSDT CNT reinforced multi-phase laminated composite plate by applying finite element method is discretized. Based on Eq. (21), one may write:

$$\begin{aligned} \int_{-\frac{h}{2}}^{\frac{h}{2}} \int_{\Omega_0} \Big\{ & \delta D_0^t(\iota_0 + z\iota_1 + z^3\iota_3 + \iota_N)^t Q_p \left(\iota_0 + z\iota_1 + z^3\iota_3 + \frac{1}{2}\iota_N\right) D_0 \\ & + \delta D_0^t(\iota_{s0} + z^2\iota_{s2})^t Q_s(\iota_{s0} + z^2\iota_{s2}) D_0 \\ & + \delta D_0^t \rho(\iota_{\theta 0} + z\iota_{\theta 1} + z^3\iota_{\theta 3})^t(\iota_{\theta 0} + z\iota_{\theta 1} + z^3\iota_{\theta 3}) D_0 \Big\} d\Omega dz - \int \int_{\Omega_0} \delta D_0^t q^{Th} d\Omega dz - \delta D_0^t F_c = 0 \end{aligned} \tag{34}$$

where $\{D_0\} = \{u_0, v_0, w_0, \phi_x, \phi_y\}^t$ is the displacement vector of a point in middle-plane, and:

$$Q_p = \begin{bmatrix} \overline{Q}_{11} & \overline{Q}_{12} & \overline{Q}_{16} \\ \overline{Q}_{12} & \overline{Q}_{22} & \overline{Q}_{26} \\ \overline{Q}_{16} & \overline{Q}_{26} & \overline{Q}_{66} \end{bmatrix}, \qquad Q_s = \begin{bmatrix} \overline{Q}_{44} & \overline{Q}_{45} \\ \overline{Q}_{45} & \overline{Q}_{55} \end{bmatrix} \tag{35}$$

$$\iota_0 = \begin{bmatrix} \frac{\partial}{\partial x} & 0 & 0 & 0 & 0 \\ 0 & \frac{\partial}{\partial y} & 0 & 0 & 0 \\ \frac{\partial}{\partial y} & \frac{\partial}{\partial x} & 0 & 0 & 0 \end{bmatrix}, \quad \iota_1 = \begin{bmatrix} 0 & 0 & 0 & \frac{\partial}{\partial x} & 0 \\ 0 & 0 & 0 & 0 & \frac{\partial}{\partial y} \\ 0 & 0 & 0 & \frac{\partial}{\partial y} & \frac{\partial}{\partial x} \end{bmatrix}, \quad \iota_2 = 0, \tag{36}$$

$$\iota_3 = \frac{-4}{3h^2}\begin{bmatrix} 0 & 0 & \frac{\partial^2}{\partial^2 x} & \frac{\partial}{\partial x} & 0 \\ 0 & 0 & \frac{\partial^2}{\partial^2 y} & 0 & \frac{\partial}{\partial y} \\ 0 & 0 & 2\frac{\partial}{\partial y}\frac{\partial}{\partial x} & \frac{\partial}{\partial y} & \frac{\partial}{\partial x} \end{bmatrix}, \quad \iota_{s0} = \begin{bmatrix} 0 & 0 & \frac{\partial}{\partial x} & 0 & 1 \\ 0 & 0 & \frac{\partial}{\partial y} & 1 & 0 \end{bmatrix}, \quad \iota_{s1} = 0,$$

$$\iota_{s2} = \frac{-4}{h^2}\begin{bmatrix} 0 & 0 & \frac{\partial}{\partial x} & 0 & 1 \\ 0 & 0 & \frac{\partial}{\partial y} & 1 & 0 \end{bmatrix}, \quad \iota_{\theta 0} = \begin{bmatrix} 1 & 0 & 0 & 0 & 0 \\ 0 & 1 & 0 & 0 & 0 \\ 0 & 0 & 1 & 0 & 0 \end{bmatrix}, \quad \iota_{\theta 1} = \begin{bmatrix} 0 & 0 & 0 & 1 & 0 \\ 0 & 0 & 0 & 0 & 1 \\ 1 & 0 & 0 & 0 & 0 \end{bmatrix},$$

$$\iota_{\theta 2} = 0, \quad \iota_{\theta 3} = -c_1\begin{bmatrix} 0 & 0 & \frac{\partial}{\partial x} & 1 & 0 \\ 0 & 0 & \frac{\partial}{\partial y} & 0 & 1 \\ 0 & 0 & 0 & 0 & 0 \end{bmatrix}, \quad \iota_N = \begin{bmatrix} 0 & 0 & \frac{\partial w_0}{\partial x}\frac{\partial}{\partial x} & 0 & 0 \\ 0 & 0 & \frac{\partial w_0}{\partial y}\frac{\partial}{\partial y} & 0 & 0 \\ 0 & 0 & \frac{\partial w_0}{\partial x}\frac{\partial}{\partial y} + \frac{\partial w_0}{\partial y}\frac{\partial}{\partial x} & 0 & 0 \end{bmatrix}$$

From the strain-displacement relationships, it is observed that the first and second-order derivatives of generalized displacements appeared in equations. Therefore, to guarantee the integrability of weak form equations, the C^1-continuity of the generalized displacement functions is generally necessary in finite element procedure. Hence, in this paper, the four-noded rectangular conforming element based on HSDT is used. The considered element is C^1-continuous with 15 DOF at each node.
The displacement vector of the reference plane based on the nodal displacement vector may be written as:

$$D_0^{(e)} = \left(\begin{array}{ccc|c|ccc} \psi_1 & \cdots & 0 & & \psi_{4y} & \cdots & 0 \\ 0 & & 0 & & 0 & & 0 \\ 0 & \ddots & 0 & \cdots & 0 & \ddots & 0 \\ 0 & & 0 & & 0 & & 0 \\ 0 & \cdots & \psi_1 & & 0 & \cdots & \psi_{4y} \end{array}\right)_{5\times 60} \quad \{d^e\} = \psi d_0^{(e)} \tag{37}$$

where:

$$\{d^e\} = \left\{ \begin{array}{c} u_{0i}, v_{0i}, w_{0i}, \phi_{xi}, \phi_{yi}, u_{0i,x}, v_{0i,x}, w_{i,x}, \\ \phi_{xi,x}, \phi_{yi,x}, u_{0i,y}, v_{0i,y}, w_{0i,y}, \phi_{xi,y}, \phi_{yi,y} \end{array} \right\}^T$$

are the 15-DOF associated with each node. The displacement interpolation functions can be written as:

$$\psi_i = \frac{1}{8}(1+\xi_i\xi)(1+\eta_i\eta)(2+\xi_i\xi+\eta_i\eta-\xi^2-\eta^2), \tag{38}$$

$$\psi_{ix} = \frac{1}{8}a\xi_i(1+\xi_i\xi)^2(1+\eta_i\eta)(\xi_i\xi-1), \tag{39}$$

$$\psi_{iy} = \frac{1}{8}b\eta_i(1+\xi_i\xi)(\eta_i\eta-1)(1+\eta_i\eta)^2, \tag{40}$$

where a and b are the half length of element in the x and y directions and the normalized coordinates are

$$\xi = \frac{x-x_c}{a}, \eta = \frac{y-y_c}{b} \tag{41}$$

where (x_c, y_c) is the center of rectangular element. Based on Eqs. (37)-(41), Eq. (34) can be expressed as:

$$\left(\delta d^{(e)}\right)^t \left\{ \int_{\Omega_0} \begin{bmatrix} \sum_{i=0}^3 B_i^t \left(Q_i^{(e)} B_0 + Q_{i+1}^{(e)} B_1 + Q_{i+3}^{(e)} B_3\right) d^{(e)} \\ + \sum_{i=0}^2 B_{si}^t \left(B_{s0} + Q_{s(i+3)}^{(e)} B_{s2}\right) d^{(e)} \\ + \sum_{i=0}^3 B_{\theta i}^t \left(I_i^{(e)} B_{\theta 0} + I_{i+1}^{(e)} B_{\theta 1} + I_{i+3}^{(e)} B_{\theta 3}\right) d^{(e)} \\ - \begin{bmatrix} B_0^t & B_1^t & B_3^t \end{bmatrix} \begin{bmatrix} q_0^{Th} \\ q_1^{Th} \\ q_3^{Th} \end{bmatrix} \end{bmatrix} d\Omega - \psi^t F_c^{(e)} \right\} = 0 \tag{42}$$

where:

$$q_i^{Th} = \int_{-h/2}^{h/2} \begin{bmatrix} \overline{Q}_{11}a_{11} + \overline{Q}_{12}a_{22} \\ \overline{Q}_{12}a_{22} + \overline{Q}_{22}a_{11} \\ \overline{Q}_{16}a_{11} + \overline{Q}_{26}a_{11} \end{bmatrix} z^i \Delta T dz \tag{43}$$

$$B_i = \iota_i \psi, \quad B_{si} = \iota_{si}\psi, \qquad B_{\theta i} = \iota_{\theta i}\psi, \quad B_N = \iota_N \psi \tag{44}$$
$$Q_i = \int_{-h/2}^{h/2} z^i Q dz, \quad Q_{si} = \int_{-h/2}^{h/2} z^i Q_s dz, \quad I_i = \int_{-h/2}^{h/2} z^i \rho dz$$

Eq. (42) holds for any arbitrary $(\delta d^{(e)})^t \neq 0$, therefore in a compact form,

$$K_L^{(e)} d_0^{(e)} + K_{NL}^{(e)} d_0^{(e)} + M^{(e)} d_0^{(e)} = F^{(e)} \tag{45}$$

where, the element stiffness matrices $K_L^{(e)}$, $K_{NL}^{(e)}$, element load vector $F^{(e)}$, element mass matrix $M^{(e)}$ can be given as:

$$\begin{aligned} K^{(e)} =& K_L^{(e)} + K_{NL}^{(e)} \\ =& \int_{\Omega_0} \left[\sum_{i=0}^{3} B_i^t \left(Q_i^{(e)} B_0 + Q_{i+1}^{(e)} B_1 + Q_{i+3}^{(e)} B_3 \right) + \sum_{i=0}^{2} B_{si}^t \left(Q_{si}^{(e)} B_{s0} + Q_{s(i+3)}^{(e)} B_{s2} \right) \right] dxdy \\ & + B_N^t \left(Q_0^{(e)} B_0 + Q_1^{(e)} B_1 + Q_3^{(e)} B_3 + \left(\frac{1}{2}\right) Q_0^{(e)} B_N \right) + \left(\frac{1}{2}\right) (B_0 + B_1 + B_3) Q_0^{(e)} B_N \end{aligned} \tag{46}$$

$$M^{(e)} = \int_{\Omega_0} \left[\sum_{i=0}^{3} B_{\theta i}^t \left(I_i^{(e)} B_{\theta 0} + I_{i+1}^{(e)} B_{\theta 1} + I_{i+3}^{(e)} B_{\theta 3} \right) \right] dxdy \tag{47}$$

$$F^{(e)} = Y^{(e)} + \psi^t F_c^{(e)} \tag{48}$$

where $Y^{(e)}$ is the element force vector:

$$Y^{(e)} = \int_{\Omega_0^{(e)}} \begin{bmatrix} B_0^t & B_1^t & B_3^t \end{bmatrix} \begin{bmatrix} q_0^{Th} \\ q_1^{Th} \\ q_3^{Th} \end{bmatrix} dxdy \tag{49}$$

Resulting time-dependent may be expressed as:

$$K\Lambda + M\ddot{\Lambda} = F \tag{50}$$

where Λ and $\ddot{\Lambda}$ are respectively the displacement and acceleration vector. K is the global stiffness matrix, includes linear and nonlinear stiffness matrix, F is the global load vector, which includes the impact force and thermal force and M is the global mass matrix.
The boundary conditions for simply supported and clamped conditions are given below:

$$u_s = w_0 = \phi_s = 0 \qquad \text{(Simply supported edge)}$$
$$u_n = u_s = w_0 = \phi_n = \phi_s = 0 \qquad \text{(Clamped edge)}$$

where the subscripts n and s denote the normal and tangential directions, respectively, on the boundaries.

In order to solve Eq. (50), Newmark's numerical time integration method is used. Based on this method, accelerations and velocities of the end of each time step are computed by (Zienkiewicz and Taylor (2005)).

$$\begin{aligned} \ddot{\Lambda}_{j+1} &= a_1(\Lambda_{j+1} - \Lambda_j) - a_2\dot{\Lambda}_j - a_3\ddot{\Lambda}_j \\ \dot{\Lambda}_{j+1} &= \dot{\Lambda}_j + a_4\ddot{\Lambda}_j + a_5\ddot{\Lambda}_j \end{aligned} \tag{51}$$

where j is the time step counter and

$$\begin{aligned} &a_1 = \frac{2}{\zeta(\Delta t)^2}; \qquad a_2 = \frac{2}{\zeta \Delta t}; \quad a_3 = \frac{1}{\zeta} - 1; \quad \zeta \leq \lambda \\ &a_4 = \Delta t(1-\lambda); \quad a_5 = \lambda \Delta t; \quad \lambda \geq 0.5 \end{aligned} \tag{52}$$

By substituting Eq. (52) into Eq. (51), we obtain

$$\hat{K}_{j+1}\Lambda_{j+1} = \hat{F}_{j+1} \tag{53}$$

where:

$$\hat{K}_{j+1} = K_{j+1} + a_1 M_{j+1} \tag{54}$$
$$\hat{F}_{j+1} = H_j M_{j+1} + F_j \tag{55}$$

Tab. 1: Material properties of the multi-phase nanocomposite plate and the impactor Shen and Zhang (2010)

Material properties of fiber (carbon)
$E_{11}^F = 233.05$ GPa, $E_{22}^F = 23.1$ GPa, $G_{12}^F = 8.96$ GPa,

$v^F = 0.2$, $\rho^F = 1750$ kg/m, $V_F = 0.6$

Material properties of epoxy matrix
$v^M = 0.34$, $\rho^M = 1150$ kg/m^3,E$^M = 2.5$ GPa

Material properties of CNT

$SWCNT$:	$MWCNT$:
E$^{CN} = 640$ GPa	E$^{CN} = 400$ GPa
d$^{CN} = 1.4 \times 10^{-9}$ m	d$^{CN} = 20 \times 10^{-9}$ m
t$^{CN} = 0.34 \times 10^{-9}$ m	t$^{CN} = 0.34 \times 10^{-9}$ m
$\rho^{CN} = 1350$ kg/m^3	$\rho^{CN} = 1350$ kg/m^3
$v_{12}^{CN} = 0.33$	$v_{12}^{CN} = 0.33$
$\ell^{CN} = 25 \times 10^{-6}$ m	$\ell^{CN} = 50 \times 10^{-6}$ m

where H_j is the following vector

$$H_j = a_1\Lambda_i + a_2\dot{\Lambda}_i - a_3\ddot{\Lambda}_j \tag{56}$$

Since Eq. (50) is a nonlinear equation, Picard or Newton-Raphson method has to be employed in each time step to reach a convergence criterion, e.g.

$$\frac{||\Lambda_i^{(\eta+1)} - \Lambda_i^{(\eta)}||}{\Lambda_i^{(\eta+1)}} \cong \Delta \tag{57}$$

where η is the iteration counter and **j** is the time step counter. Δ is a sufficiently small number.

4 Results and discussions

In present section, after validation of the results, the effects of the weight percentage of SWCNTs and MWCNTs, nanotube aspect ratio, volume fraction of fibers, plate aspect ratio and initial velocity of the impactor on the contact force, indentation, and central deflection of CNT reinforced multi-phase laminated composite plate are studied in details. Since the numerical time integration procedures manifest an error accumulation phenomenon that is especially affected by the time integration steps and in order to trace the time history of the quantities more adequately, the integration time steps have to be much less than the fundamental period time of the structure, and especially much less than the response time of the structure. For this reason, a time step that is equal or less than 10^{-6} (sec) is adopted. Also $\Delta = 0.0001$ is used for the convergence criterion Eq. (50).
In present section, response of a laminated fully clamped, symmetric cross ply, CNT reinforced multi-phase laminated composite plate subjected to nonlinear low-velocity impact is investigated. A plate with dimensions of $0.2 \times 0.2 \times 0.02$ (m) and the stacking sequence $\{0/90/90/0\}$ is considered. Material properties of the plate is presented in Table 1. The impactor is made from steel with radius $R = 6.35$ mm, and initial velocity $V_0 = 3$ m/s, material properties of $E_i = 207$ GPa, $\nu_i = 0.3$ and $\rho_i = 7960$ kg/m^3.
Effect of weight percentage of CNT on the nonlinear low-velocity impact response of a multi-phase laminated composite plate reinforced with SWCNT and MWCNT are depicted in Figs. 2 and 3. Four different weight percentage, $w_{CN} = 0\%$, $w_{CN} = 1\%$, $w_{CN} = 2\%$ and $w_{CN} = 3\%$ are considered. Since increasing the weight percentage increases percentage of CNT at the contact region, it leads to an increased contact stiffness and the peaks of the contact force history and a decreased peak indentation. Increasing the CNT's weight percentage leads to a plate with higher bending rigidity and subsequently, higher natural frequencies and smaller response times. Due to this reason, the contact time duration and central deflection has decreased with increasing the weight percentage. Further the effect of weight percentage of is more prominent in SWCNTs reinforced composite plates rather than MWCNTs reinforced composite plates.
Figs. 4 and 5 shows the effect of aspect ratio of CNT on the contact force, indentation, and central deflection of fully clamped, symmetric cross ply, SWCNT and MSCNT reinforced multi-phase laminated composite plate respectively. Six sets of aspect ratios have been considered here, i.e., $\ell^{CN}/d^{CN} = 100$; $\ell^{CN}/d^{CN} = 200$; $\ell^{CN}/d^{CN} = 500$; $\ell^{CN}/d^{CN} = 1000$; $\ell^{CN}/d^{CN} = 2000$ and $\ell^{CN}/d^{CN} = 10000$. As may be noted, composite plate reinforced with longer CNTs has more stiffening behavior and as the aspect ratio of CNT increases the peaks of central deflection decreases whereas indentation and contact force increases and the peak contact force and deflection are achieved in earlier time instants. It should be noted that for aspect ratios higher than $500(\ell^{CN}/d^{CN} > 500)$ this influence is insignificant. Fig. 6 depicts the variation of maximum impact force, indentation and central deflection of fully clamped, symmetric cross ply, SWCNT and MWCNT reinforced multi-phase laminated composite plate with nanotube aspect. As Fig. 6 reveals, contact time and maximum central deflection decrease while increases the maximum contact force of SWCNT reinforced composites rapidly with increase of CNT aspect ratio up to 500 and thereafter it is almost constant. Whereas, no significant change in the response of MWCNT reinforced composite plate subjected to nonlinear low-velocity impact is observed when aspect ratio of CNT increases.

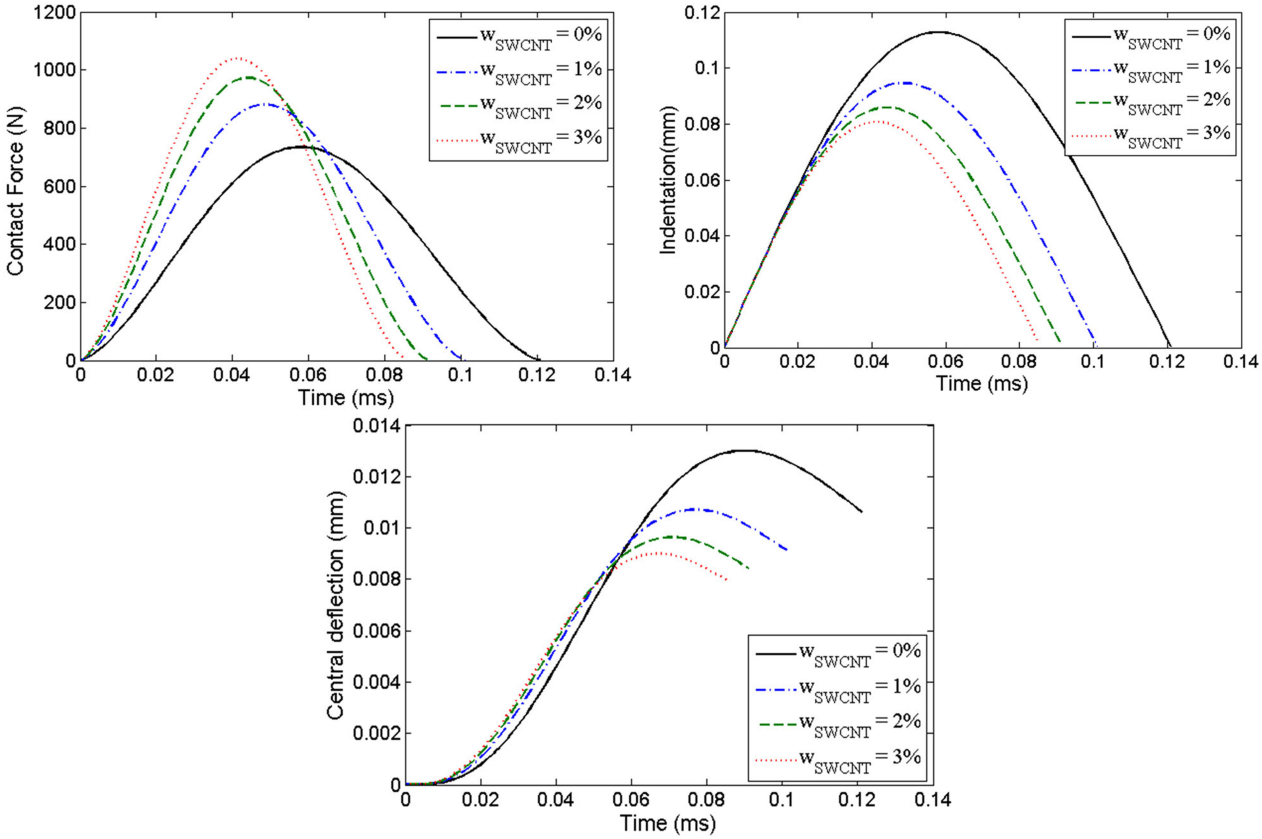

Fig. 2: Effect of the weight percentage of SWCNTs on the impact responses of plate. (From top-left clockwise)(a) Contact force; (b) indentation, (c) central deflection of plate

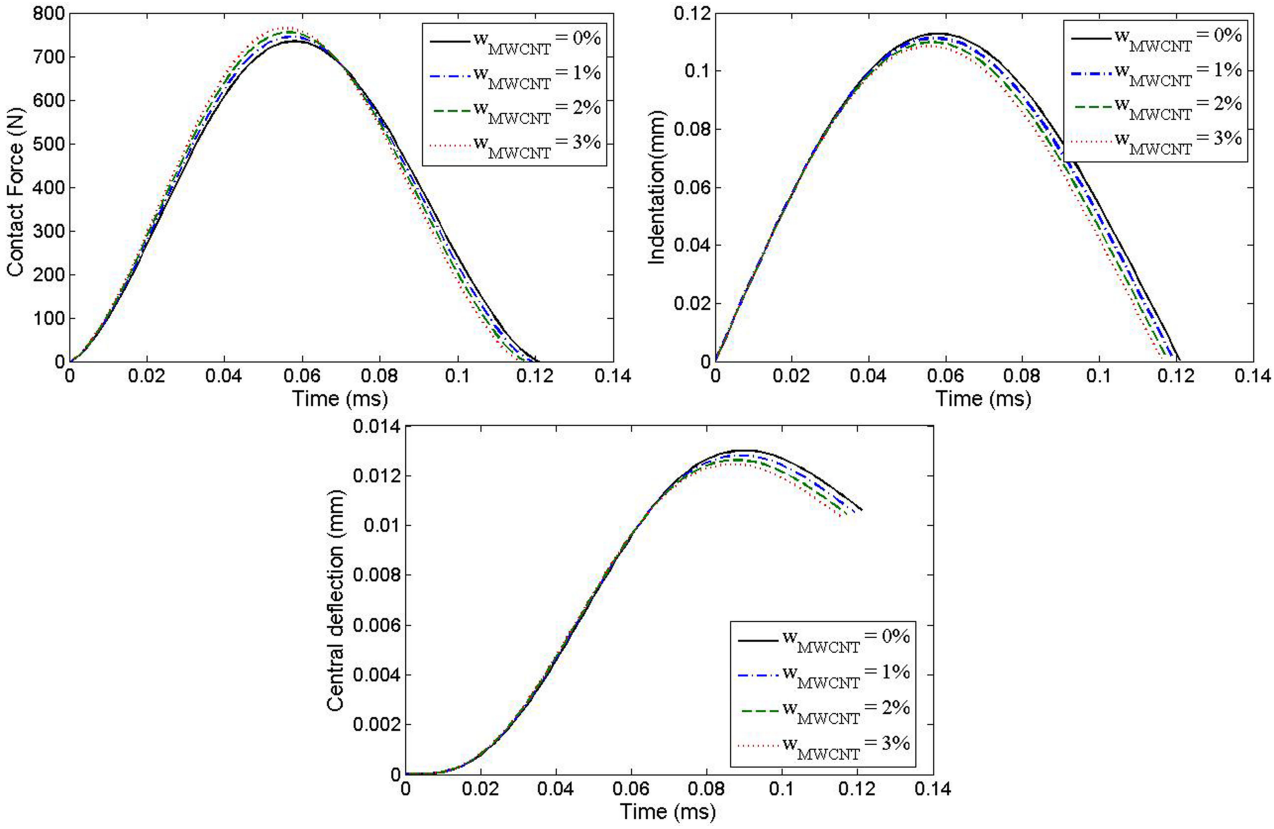

Fig. 3: Effect of the weight percentage of MWCNTs on the impact responses of plate. (From top-left clockwise)(a) Contact force; (b) indentation, (c) central deflection of plate

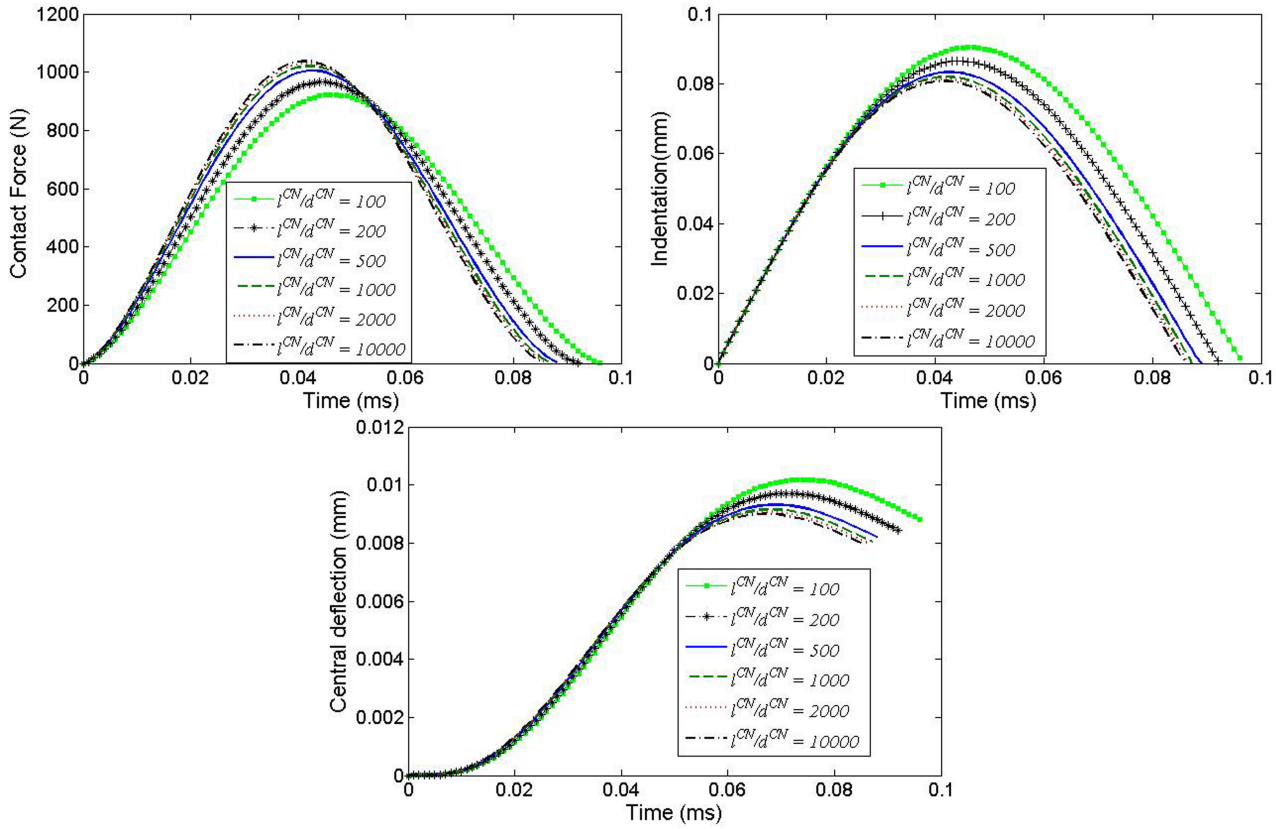

Fig. 4: Effect of SWCNTs aspect ratio on the impact responses of plate. (From top-left clockwise)(a) Contact force; (b) indentation, (c) central deflection

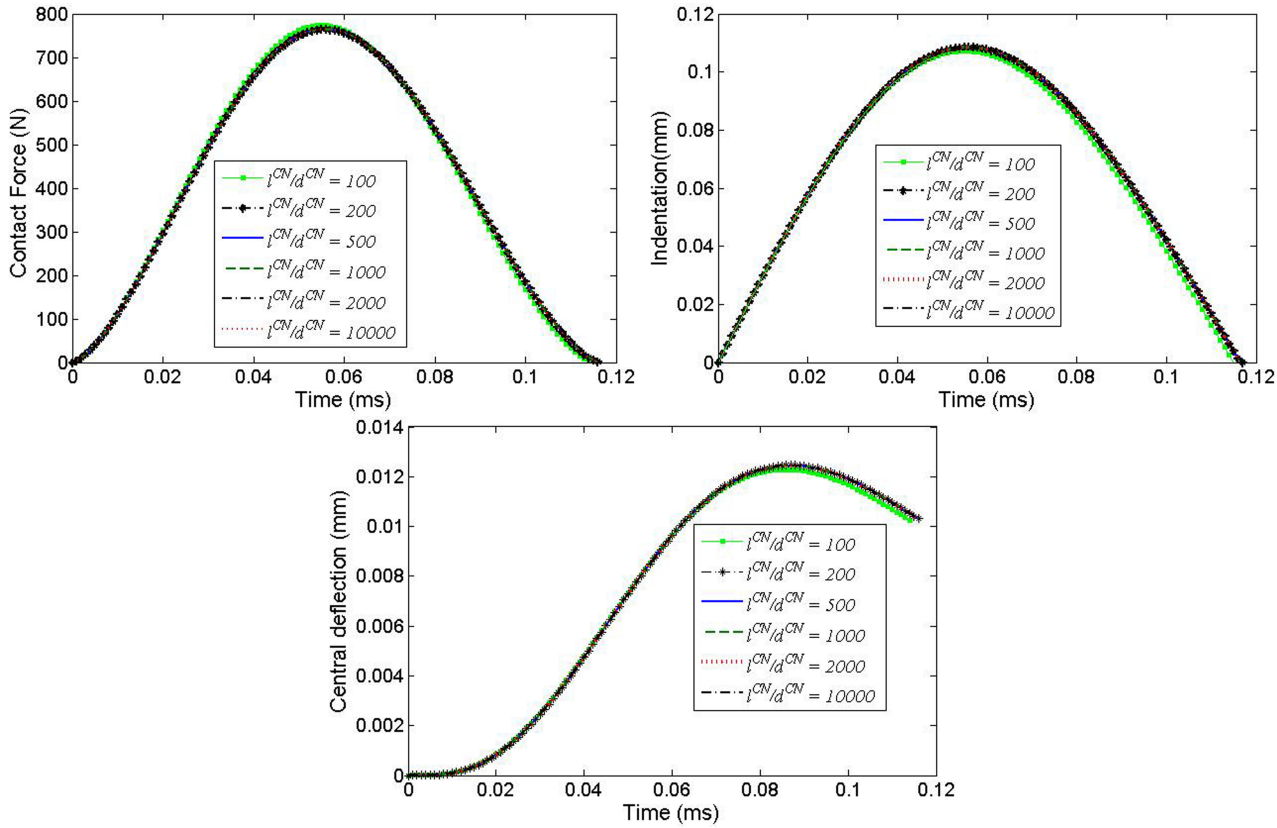

Fig. 5: Effect of MWCNTs aspect ratio on the impact responses plate. (From top-left clockwise) (a) Contact force; (b) indentation, (c) central deflection

5 Conclusion

Response of CNT reinforced multi-phase laminated composite plate subjected to nonlinear low-velocity impact using the finite element method is performed. The four-noded rectangular conforming element with 15 DOF at each node based on HSDT

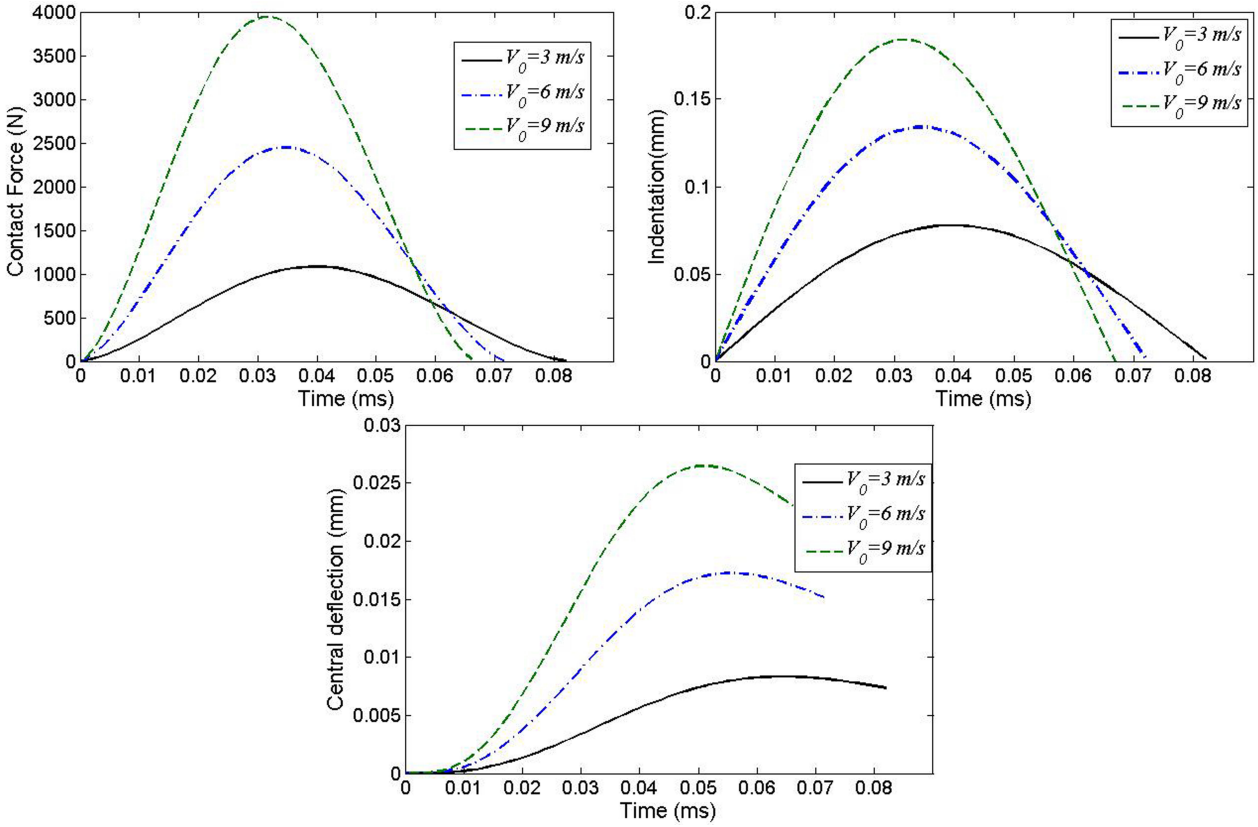

Fig. 6: Effect of initial velocity on the impact responses of plate. (From top-left clockwise) (a) Contact force; (b) indentation, (c) central deflection

and C^1-continuity of the generalized displacement functions is employed. The effective material properties of the multi-phase nanocomposite are calculated using Halpin-Tsai equations and fiber micromechanics in hierarchy. Contact force between the impactor and the laminated plate is obtained with the aid of the modified nonlinear Hertzian contact law models. Results are to explore the effects of various parameters. It is concluded that:

- A small amount of CNT (1-2 percent) can increase the maximum contact and decrease the maximum indentation. Also the contact time duration and central deflection has decreased with increasing the CNT percentage.
- SWCNT reinforcement produces more pronounced effect on the low velocity impact of the plate in comparison to MWCNT. It may be attributed to the defect free structure of SWCNT.
- CNT aspect ratio play a significant role influencing the impact behavior, but only for SWCNT reinforced composite plates. It should be noted that for composite plate reinforced with short CNT (aspect ratio less than 50) this influence is insignificant.
- Contact time and maximum central deflection decrease while increases the maximum contact force of SWCNT reinforced composite rapidly with increase of CNT aspect ratio up to 500 and thereafter it is almost constant.
- Effect of CNT reinforcement is more prominent in thick plates rather than in thin plates.

References

B. Akgoz and O. Civalek. Buckling analysis of linearly tapered micro-columns based on strain gradient elasticity. *Structural Engineering and Mechanics*, 48(2):195–205, 2013.

E. Bekyarova, E. T. Thostenson, A. Yu, H. Kim, J. Gao, J. Tang, H. T. Hahn, T. W. Chou, M. E. Itkis, and R. C. Haddon. Multiscale carbon nanotube-carbon fiber reinforcement for advanced epoxy composites. *Langmuir*, 23:3970–3974, 2007.

G. Bhardwaj, A. K. Upadhyay, R. Pandey, and K. K. Shukla. Non-linear flexural and dynamic response of cnt reinforced laminated composite plates. *Compos. Part B: Eng.*, 45:89–100, 2012.

C. Demir, K. Mercan, and O. Civalek. Determination of critical buckling loads of isotropic, fgm and laminated truncated conical panel. *Composites Part B*, 94:1–10, 2016.

F. Ebrahimi, Ali Jafari, and R. Selvamani. Thermal buckling analysis of magneto electro elastic porous fg beam in thermal environment. *Advanes in Nano Research*, 8(1):83–94, 2020a.

F. Ebrahimi, Mahsa Karimiasl, and R. Selvamani. Bending analysis of magneto-electro piezoelectric nanobeams system under hygro-thermal loading. *Advanes in Nano Research*, 8(3):203–214, 2020b.

F. Ebrahimi, Mohammadreza Kokaba, Gholamreza Shaghaghi, and R. Selvamani. Dynamic characteristics of hygro-magneto-thermo-electrical nanobeam with non-ideal boundary conditions. *Advanes in Nano Research*, 8(2):169–182, 2020c.

F. S. Ebrahimi, Hamed Hosseini, and R. Selvamani. Thermo-electro-elastic nonlinear stability analysis of viscoelastic double-piezo nanoplates under magnetic field. *Structural Engineering and Mechanics*, 73(5):565–584, 2020d.

Farzad Ebrahimi, Erfan Salari, and Seyed Amir Hosein Hosseini. Thermomechanical vibration behavior of fg nanobeams subjected to linear and non-linear temperature distributions. *Journal of Thermal Stresses*, 38(12):1360–1386, 2015.

A. Godara, L. Mezzo, F. Luizi, F. Warrier, S. V. Lomov, A. W. V. Vuure, L. Gorbatikh, P. Moldenaers, and I. Verpoest. Influence of carbon nanotube reinforcement on the processing and the mechanical behavior of carbon fiber/epoxy composites. *Carbon*, 47:2914–2923, 2009.

K. J. Green, R. D. Derrick, K. V. Uday, and N. Elijah. Multiscale fiber reinforced composites based on a carbon nanofiber/epoxy nano phased polymer matrix: synthesis, mechanical and thermo mechanical behavior. *Composites Part A. App. Sci. Manuf.*, 40:1470–1475, 2009.

M. Gurses, O. Civalek, A. Korkmaz, and H. Ersoy. Free vibration analysis of symmetric laminated skew plates by discrete singular convolution technique based on first-order shear deformation theory. *International journal for numerical methods in engineering*, 79(3):290–313, 2009.

X. Q. He, M. Rafiee, S. Mareishi, and K. M. Liew. Large amplitude vibration of fractionally damped viscoelastic cnts/fiber/polymer multiscale composite beams. *Compos Struc*, 131:1111–1123, 2015.

J. E. Jam and Y. Kiani. Low velocity impact response of functionally graded carbon nanotube reinforced composite beams in thermal environment. *Compos. Struct.*, 132:35–43, 2015.

M. Kim, Y. Park, O. Okoli, and C. Zhang. Processing, characterization, and modeling of carbon nanotube-reinforced multiscale composites. *Compos Sci Tech*, 69:335–42, 2009.

V. Kostopoulos, A. Baltopoulos, P. Karapappas, A. Vavouliotis, and A. Paipetis. Impact and after-impact properties of carbon fibre reinforced composites enhanced with multi-wall carbon nanotubes. *Compos. SciTechnol*, 70:553–63, 2010.

M. Mura. *Micromechanics of Defects in Solids*. Academic, Dordrecht: Kluwer, 1987.

M. Rafiee, J. Yang, and S. Kitipornchai. Large amplitude vibration of carbon nanotube reinforced functionally graded composite beams with piezoelectric layers. *Compos. Struct.*, 96:716–725, 2013.

M. Rafiee, X. Q. He, S. Mareishi, and K. Liew. Modeling and stress analysis of smart cnts/fiber/polymer multiscale composite plates. *Int. J. App. Mech.*, 6:1450025, 2014a.

M. Rafiee, X. F. Liu, X. Q. He, and S. Kitipornchai. Geometrically nonlinear free vibration of shear deformable carbon nanotube/fiber/polymer multiscale laminated composite plates. *J. Sound Vibr.*, 333(14):3236–3251, 2014b.

R. Rafiee and R. M. Moghadam. Simulation of impact and post-impact behavior of carbon nanotube reinforced polymer using multi-scale finite element modeling. *Comput. Mater. Sci.*, 63:261–268, 2012.

M. Rahman, M. Hosur, K. T. Hsiao, L. Wallace, and S. Jeelani. Low velocity impact properties of carbon nanofibers integrated carbon fiber/epoxy hybrid composites manufactured by ooa-vbo process. *Compos. Struct.*, 120:32–40, 2015.

J. N. Reddy. *Mechanics of laminated composite plates and shells: theory and analysis*. CRC Press, 2 edition, 2004.

N. G. Sahoo, S. Rana, J. W. Cho, L. Li, and S. H. Chan. Polymer nanocomposites based on functionalized carbon nanotubes. *Prog. Polym. Sci.*, 35:837–67, 2010.

R. Selvamani and F. Ebrahimi. Axisymmetric vibration in a submerged, piezoelectric rod coated with thin film. *Trends in Mathematics*, 2020.

A. R. Setoodeh, P. Malekzadeh, and K. Nikbin. Low velocity impact analysis of laminated composite plates using a 3d elasticity based layerwise fem. *Mater Des.*, 30(9):3795–801, 2009.

H. S. Shen. A comparison of buckling and postbuckling behavior of fgm plates with piezoelectric fiber reinforced composite actuators. *Compos. Struct.*, 91:375–384, 2009.

H. S. Shen and C. L. Zhang. Thermal buckling and postbuckling behavior of functionallygraded carbon nanotube-reinforced composite plates. *Mater Des.*, 31:3403–11, 2010.

M. E. Soliman, P. M. Sheyka, and M. R. Taha. Low-velocity impact of thin woven carbon fabric composites incorporating multi-walled carbon nanotubes. *Int. J. Impact Eng.*, 47:39–47, 2012.

Z. Spitalsky, D. Tasis, K. Papagelis, and Galiotis C. Carbon nanotube-polymer composites: Chemistry, processing, mechanical and electrical properties. *Prog. Polym. Sci.*, 35(3):357–401, 2010.

C. T. Sun and J. K. Chen. On the impact of initially stressed composite laminates. *J. Comput. Math.*, 19(11):490–504, 1985.

L. X. Sun and T. R. Hsu. Thermal buckling of laminated composite plates with transverse shear deformation. *Comput. Struc.*, 36:883–89, 1990.

M. Talebitooti. Three-dimensional free vibration analysis of rotating laminated conical shells: layerwise differential quadrature (lw-dq) method. *Arch. Appl. Mech.*, 83:765–781, 2013.

E. T. Thostenson, Z. H. Ren, and T. W. Chou. Advances in the science and technology of carbon nanotubes and their composites: a review. *Compos. Sci. Techno.*, 16(13):1899–1912, 2001.

E. T. Thostenson, W. Z. Li, D. Z. Wang, Z. F. Ren, and T. W. Chou. Carbon nanotube/carbon fiber hybrid multi scale composites. *J. App. Phys.*, 91:6034–6037, 2002.

Z. X. Wang, J. Xu, and P. Qiao. Nonlinear low-velocity impact analysis of temperature-dependent nanotube-reinforced composite plates. *Compos. Struct.*, 108:423–34, 2014.

S. H. Yang and C. T. Sun. Indentation law for composite laminates. In *Composite materials: testing and design (6th conference)*, volume 5, pages 425–49. ASTM STP-787, 1982.

O. C. Zienkiewicz and R. L. Taylor. *The finite element method: its basis and fundamentals*. Butterworth-Heinemann, 6 edition, 2005.